Supplement of Atmos. Meas. Tech. Discuss., 8, 4653–4709, 2015
http://www.atmos-meas-tech-discuss.net/8/4653/2015/
doi:10.5194/amtd-8-4653-2015-supplement

Atmospheric Measurement Techniques Discussions

Supplement of

Cloud and aerosol classification for 2 1/2 years of MAX-DOAS observations in Wuxi (China) and comparison to independent data sets

Y. Wang et al.

Correspondence to: Y. Wang (y.wang@mpic.de)

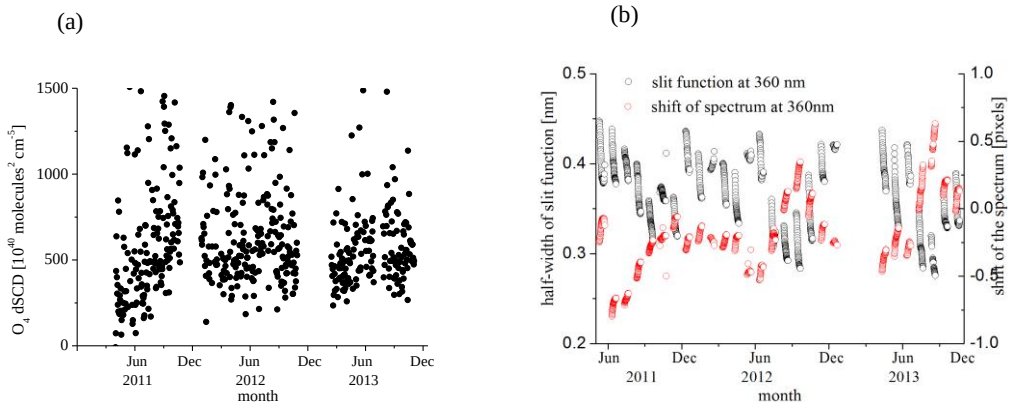

Fig. S1 (a): O_4 dSCD for zenith view in the SZA range of 49 ° to 51 ° from the retrievals with a fixed reference spectrum (from Sep 15, 2012). (b): The full width at half maximum and spectral shift (red points) of the measured spectra derived from a fit to a high-resolution solar spectrum.

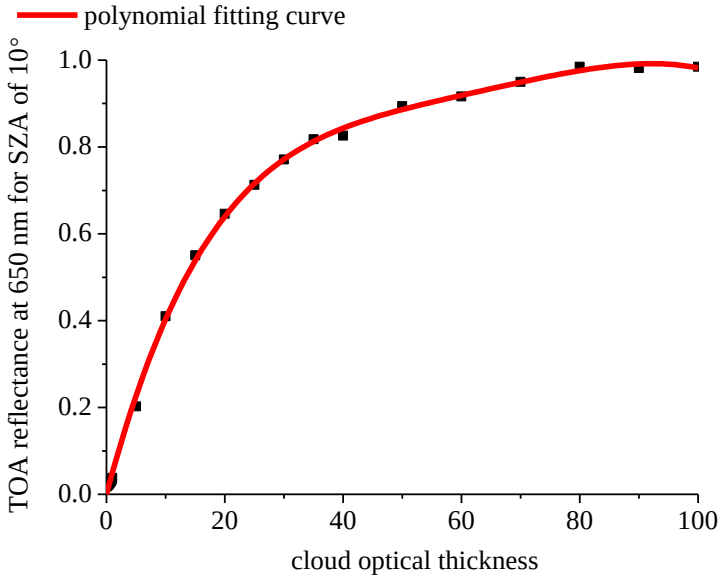

Fig. S2 Top of the atmosphere (TOA) reflectance at 650 nm for nadir view for SZA of 10 ° as a function of the cloud optical thickness derived from radiative transfer simulations. The cloud optical properties are described by the Henyey Greenstein approximation with an asymmetry parameter of 0.85 and a single scattering albedo of 1. The cloud layer range is from 1 to 2 km for COT of 1 to 15, from 1 to 3 km for COT of 20 to 30, from 1 to 4 km for COT of 35 to 40, and from 1 to 5km for COT of 50 to 100.

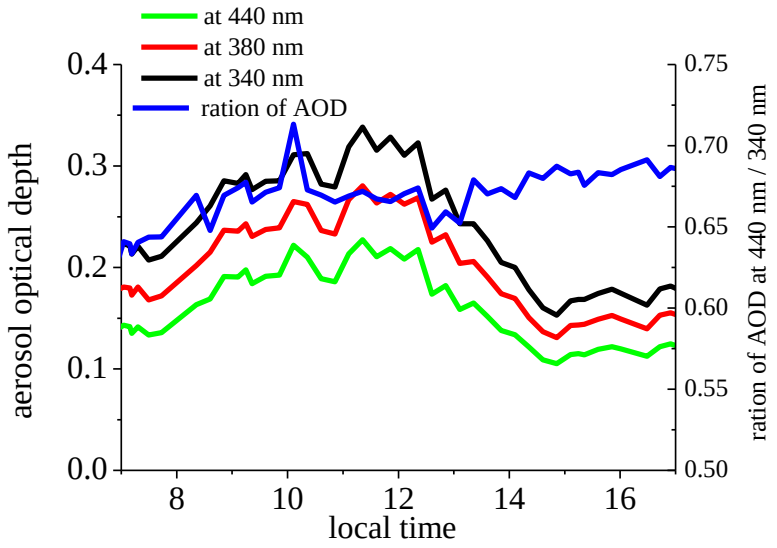

Fig. S3 Time series of the AOD at 340 nm (black), 380 nm (red) and 440 nm (green) on 29 July 2012 as well as the ratio of the AOD at 440 and 340 nm (black) (right axis) in the sky condition of "extremely high midday CI".

Comparison of cloud products from MODIS, OMI and GOME-2

We briefly discuss the satellite cloud products in more detail and compare them with each other. Here we make use of the fact that the overpass time of MODIS on Terra is similar to that of GOME-2, and the overpass time of MODIS on Aqua is similar to that of OMI to compare the cloud products from GOME-2 and OMI with MODIS.

In Fig. S4a the effective CFs from OMI are compared with the corresponding MODIS results (on Aqua). Because the effective CF is clipped between 0 and 1, we excluded the data with effective CF of 100% and smaller than 1% for this comparison. A good agreement with the fitted linear slope of 0.71, the intercept of 6.7% and the square of correlation coefficient (R^2) of 0.61 is found. The different spatial resolution

and slightly different overpass time of the two instruments contribute to the scattering of the points. The different retrieval techniques may also contribute to the discrepancy of effective CFs between both satellite instruments. In Fig. S4b in the same way the effective CFs from GOME-2 are compared with the corresponding MODIS results (on Terra). A good agreement with the fitted linear slope of 0.86, the intercept of 14% and the R^2 of 0.61 is found. The larger effective CF from GOME-2 than that from MODIS is found, especially when the COT is low. This phenomenon has been found by Acarreta et al. (2004). Besides different spatial resolution and overpass time, the different spatial collocation criteria of GOME-2 and MODIS also contribute to the discrepancy between them.

The retrieval algorithms using the O_4 absorption for OMI and the O_2 (FRESCO+) for GOME-2 normally retrieve much larger CP than MODIS, especially for optically thick clouds. The reason is that multiple scattering leads to the fact that the cloud pressure from the O_4 absorption algorithm and FRESCO+ is closer to the middle of the clouds than to the top of the clouds (Acarreta et al., 2004; Wang et al., 2008; Wang and Stammes, 2014). The comparisons of the CPs from OMI and GOME-2 with those from MODIS in Fig. S4c and d also show the same feature.

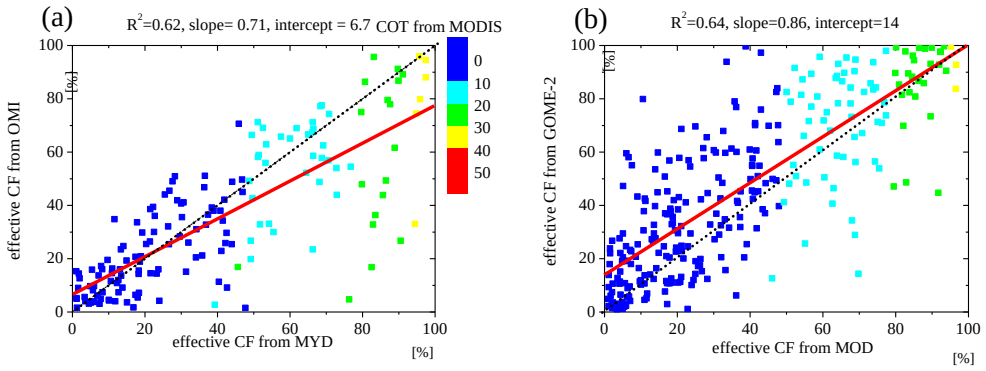

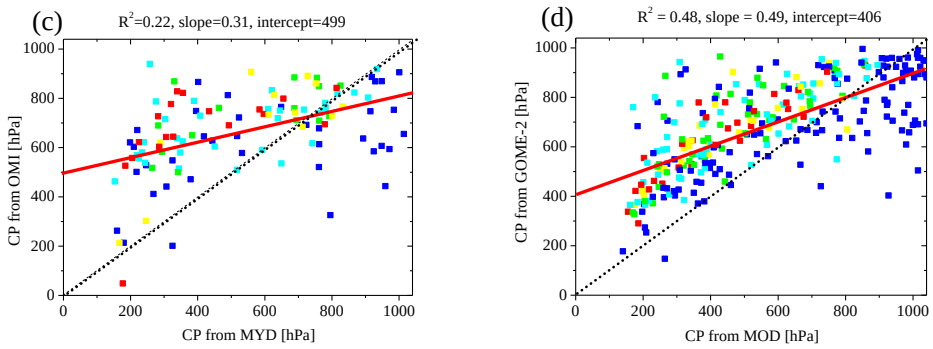

Fig. S4 Comparison of cloud products derived from GOME-2 or OMI and MODIS: effective CF from OMI and GOME-2 are plotted against those from MODIS on Aqua (MYD) a) and on Terra (MOD) b), respectively; CPs from OMI and GOME-2 are plotted against those from MODIS on Aqua (MYD) c) and on Terra (MOD) d), respectively. The black dashed line indicates the 1:1 line. The colours indicate the COT from MODIS. The comparisons are performed for satellite measurements over the Wuxi site. For the comparison of CPs, the data with corresponding effective CF < 20% are excluded to only keep the cloudy conditions, because the CP can't be accurately retrieved for effective CF < 20%.

Selection of threshold values

The procedure for the selection of threshold values is described. Firstly the days with specific sky conditions were selected based on visual images from MODIS (Fig. S5), time series of AOD at 340 nm from Aeronet (Fig. S6a), and the visibility at 550 nm derived from the visibility meter (Fig. S6b):

-24 September 2012: clear sky with low aerosol

-29 September 2012: clear sky with high aerosol

-20 July 2012: broken clouds

-9 September 2012: continuous and thick clouds (the COT from MODIS is around 50)

-28 July 2012: cloud holes

-10 June 2012: fog

Fig. S7 depicts the time series of the quantities described in Table 1 for the six selected days. From visible inspection of the different quantities for the different sky conditions on the selected days we determined the respective threshold values, which are listed in Table 1. In Fig. S8 exemplary results of the cloud classification scheme are presented for the selected days (including also the days shown in Figs. 7 and 8 of the main manuscript). Overall the deduced sky conditions are consistent with those identified by the MODIS images, and the measurements from AERONET and the visibility meter.

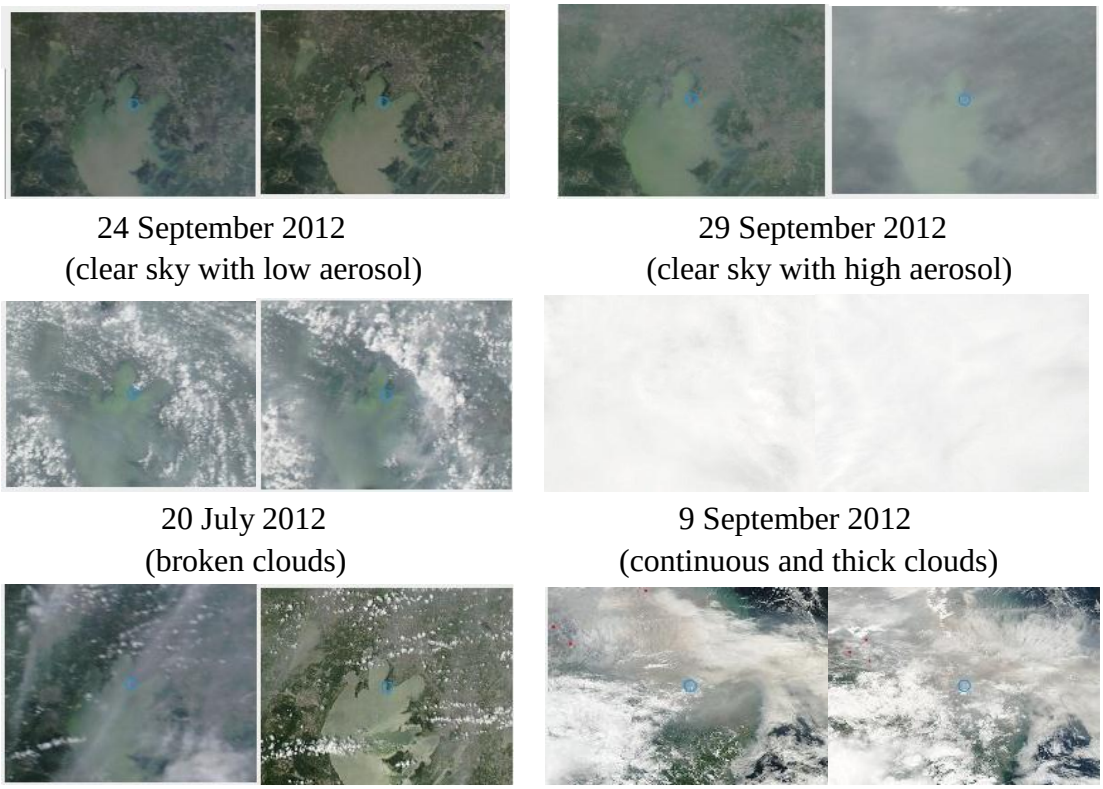

24 September 2012 (clear sky with low aerosol)

29 September 2012 (clear sky with high aerosol)

20 July 2012 (broken clouds)

9 September 2012 (continuous and thick clouds)

28 July 2012 (cloud holes)

10 June 2012 (fog)

Fig. S5 Visual images from MODIS (left Terra; right: Aqua) for the six selected days with different sky conditions near Wuxi.

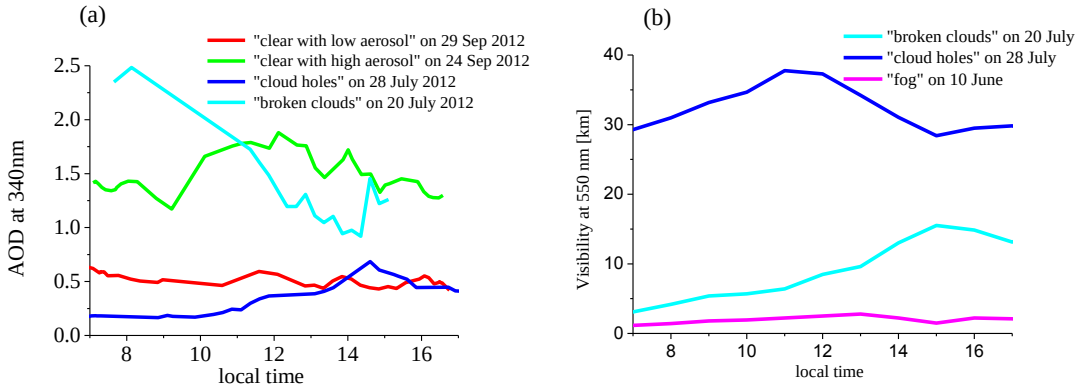

Fig. S6 (a) Time series of the AOD at 340 nm from AERONET on the days with clear sky, cloud holes or broken clouds (AOD data are not available for the other days because of clouds); (b) Time series of the visibility at 550 nm from the visibility meter on the days with broken clouds, cloud holes and fog (visibility data are not available for the other days due to instrumental problems).

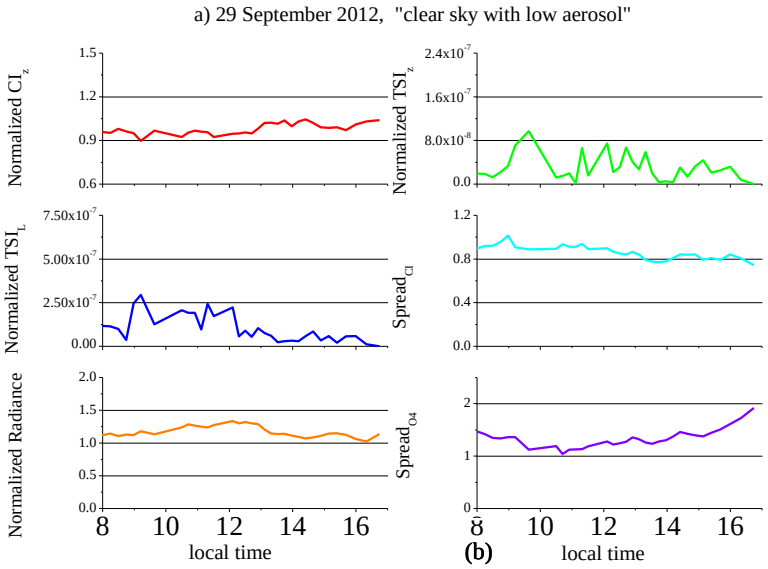

b) 24 September 2012, "clear sky with high aerosol"

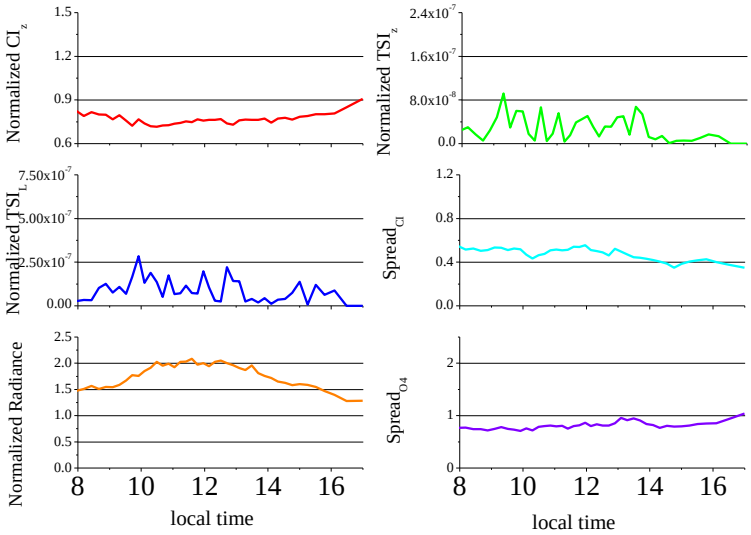

c) 20 July 2012, "broken clouds"

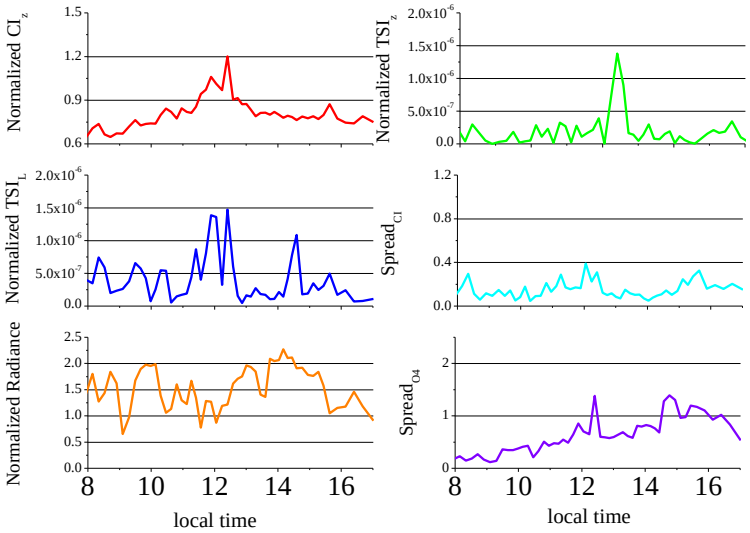

d) 9 September 2012, "continuous clouds"

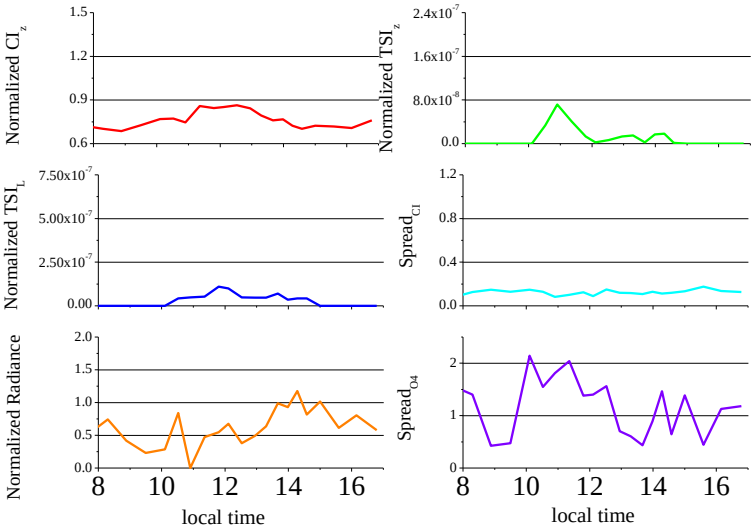

e) 28 July 2012, "cloud holes"

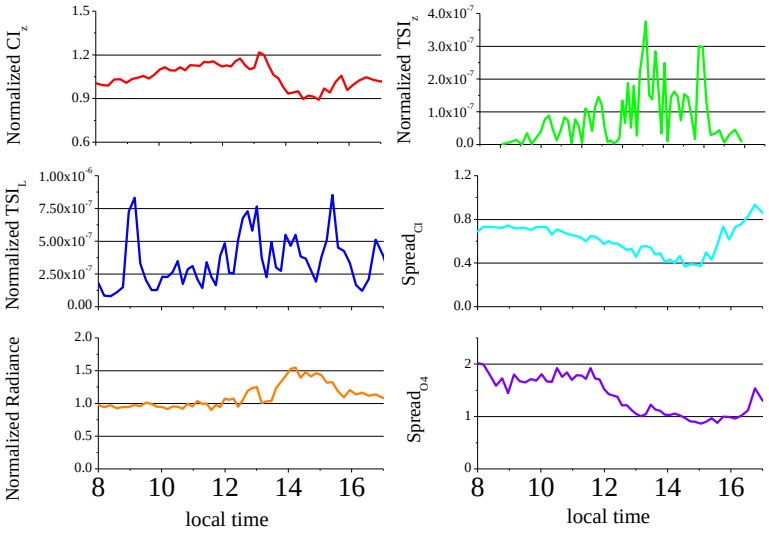

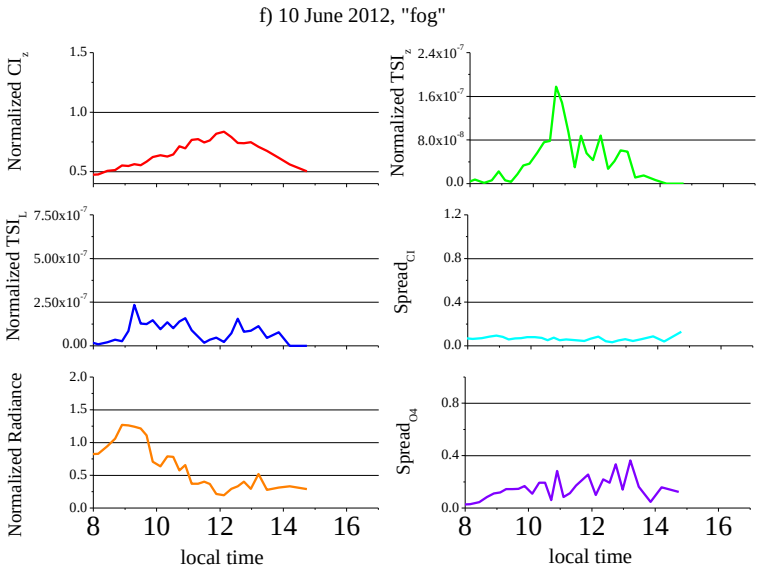

Fig. S7 Time series of the normalized Cl_z, normalized TSI_z, normalized TSI_L, $spread_{Cl}$, normalized radiance and $spread_{O4}$ on the six selected days with the typical different sky conditions.

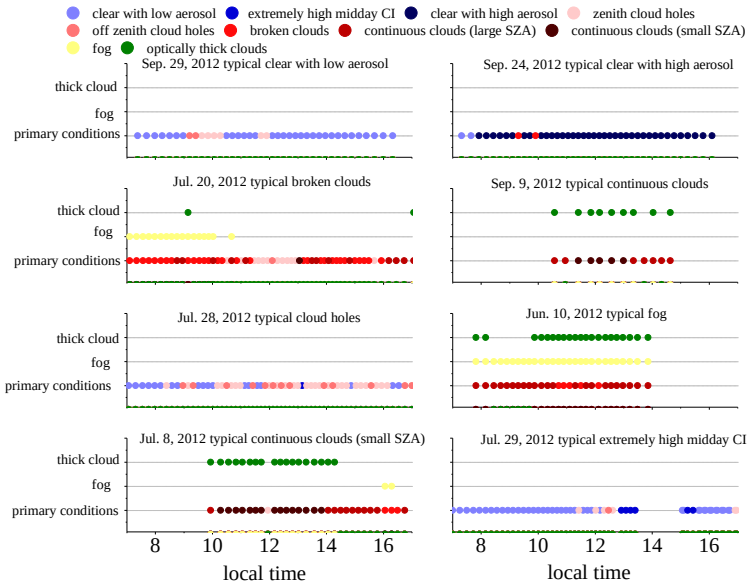

Fig. S8 Results of the cloud classification scheme for the selected days. Each symbol represents an individual elevation sequence. In the lower part of the indiviual figures, the primary sky conditions are indicated. In both upper parts the secondary sky conditions ‘optically thick clouds’ and ‘fog’ are indicated.